

An experimental approach to determine the heat transfer coefficient in directional solidification furnaces

Mohsen Banan, Ross T. Gray and William R. Wilcox

Center for Crystal Growth in Space and School of Engineering, Clarkson University, Potsdam, New York 13699, USA

Received 13 November 1990; manuscript received in final form 22 April 1991

The heat transfer coefficient between a molten charge and its surroundings in a Bridgman furnace was experimentally determined using in-situ temperature measurement. The ampoule containing an isothermal melt was suddenly moved from a higher temperature zone to a lower temperature zone. The temperature-time history was used in a lumped-capacity cooling model to evaluate the heat transfer coefficient between the charge and the furnace. The experimentally determined heat transfer coefficient was of the same order of magnitude as the theoretical value estimated by standard heat transfer calculations.

1. Introduction

A variety of directional solidification techniques are used for preparation of materials, especially for growth of single crystals. These techniques include the vertical Bridgman-Stockbarger, horizontal Bridgman, zone-melting, and gradient freeze methods. It is time consuming and costly to experimentally determine the optimal thermal conditions of a furnace utilized to grow a specific material. Hence, it is desirable to employ analytical and numerical models to assist in determining the optimal thermal conditions for a specific growth system, e.g. vertical Bridgman-Stockbarger technique [1-6]. Such calculations are handicapped by limited knowledge of the growth environment's thermal characteristics.

The heat transfer coefficient, defined as the ratio of the heat flux to the temperature difference between the material and the furnace, is an important thermal parameter in a growth system. The heat transfer coefficient manifests itself in the heat transfer models as the Biot number hR/k , where h is the heat transfer coefficient, R is the sample radius, and k is the thermal conductivity of the sample. The Biot number may be regarded as the ratio of the ease of heat exchange with the furnace to heat conduction through the charge.

Chang and Wilcox [1] showed that increasing the Biot number in Bridgman growth affects the position and shape of the isotherms in the furnace. The sensitivity of interface position to the hot and cold zone temperatures is greater for small Biot number.

Fu and Wilcox [2] showed that decreasing the Biot numbers in the hot and cold zones of a vertical Bridgman-Stockbarger system results in isotherms becoming less curved. The planar isotherms lie in the lower portion of the adiabatic zone when the heater's Biot number is larger than the cooler's Biot number. Increasing the cooler's Biot number moved the position of the planar interface toward the upper section of the adiabatic zone.

Although the heat transfer coefficient may be estimated from heat transfer principles [5,7], considerable uncertainties make an experimental value preferred. We report an experimental approach to determine the average heat transfer coefficient between the growth material and the furnace. This is accomplished by in-situ temperature measurement of a transiently cooled object, i.e. melt or solid contained in an ampoule. In this technique, an isothermal charge at temperature T_0 is suddenly moved to a chamber at temperature T_∞ . The temperature of the charge is measured as a function of

time with a thermocouple. The data obtained are used in a lumped-capacity model to calculate the average heat transfer coefficient between the molten charge and its surroundings. A GaSb charge was used to demonstrate the method. The validity of the lumped-capacity model was examined by use of the one-dimensional transient heat transfer problem between a rod and its surroundings and comparing the results of this analysis with the lumped-capacity solution. The one-dimensional transient problem considers radial temperature gradients in the rod.

2. Lumped-capacity model

The value of the heat transfer coefficient depends on the geometry of the system as well as the physical properties and temperatures of the material and its environment. A simple, but important method, based on a lumped-capacity solution [8] can be used to determine the average heat transfer coefficient between an object and its surroundings from the transient cooling of the object. The analysis assumes that the object is isothermal. This object at temperature T_0 is introduced suddenly into an environment at temperature T_∞ . The heat transfer coefficient is calculated from the change in temperature of the object as a function of time. The analytical development of the lumped-capacity model is presented in ch. 4, pp. 101–108, of Ozisik [8]. The temperature–time relationship is given in non-dimensional form as:

$$\ln \theta = (-2 \text{Bi}) \tau, \quad (1)$$

where $\text{Bi} = \bar{h}R/k$, $\theta = (T - T_\infty)/(T_0 - T_\infty)$, $\tau = \alpha t/R^2$, and α is the thermal diffusivity of the object. The Biot number is found from the slope of a $\ln \theta$ versus τ plot and the heat transfer coefficient is given by:

$$\bar{h} = \text{Bi} k/R. \quad (2)$$

In our experiments, the object consisted of a molten GaSb charge contained in a quartz ampoule (discussed in detail in the experimental section). The environment was a vertical Bridgman–Stockbarger furnace. The ampoule wall added a

resistance to the heat transfer between the charge and the furnace. To include the effect of such resistance on the heat transfer coefficient, some modifications of the thermophysical properties in eqs. (1) and (2) were necessary. (A similar approach was undertaken by Naumann [5].) The mass weighted effective thermal conductivity and thermal diffusivity are defined as follows:

$$k_{\text{eff}} = \frac{\rho_c V_c k_c + \rho_a V_a k_a}{\rho_c V_c + \rho_a V_a}, \quad (3)$$

$$\alpha_{\text{eff}} = \frac{k_{\text{eff}}}{\rho_{\text{avg}} c_{\text{eff}}} = \frac{(\rho_c V_c k_c + \rho_a V_a k_a)(V_c + V_a)}{(\rho_c V_c c_c + \rho_a V_a c_a)(\rho_c V_c + \rho_a V_a)}, \quad (4)$$

where all parameters are defined in the table of nomenclature. The effective heat transfer coefficient then becomes:

$$\bar{h}_{\text{eff}} = \text{Bi}_{\text{eff}} k_{\text{eff}}/R_a, \quad (5)$$

where R_a is the outer radius of the ampoule and Bi_{eff} is found from the slope of the $\ln \theta$ versus $\tau_{\text{eff}} = \alpha_{\text{eff}} t/R_a^2$ plot.

3. Validity of the lumped-capacity model

In order to determine the validity of the lumped-capacity model for different ranges of the Biot number, a similar model was solved which takes radial temperature gradients in the sample into account. This model assumes that the heat flow is axisymmetric, the temperature in the rod is uniform in the axial direction, and the density, specific heat, and thermal conductivity of the rod are independent of temperature. It is valid for all values of the Biot number. The solution to this problem is given in ch. 7, pp. 201–202, of Carslaw and Jaeger [9]. When this solution is simplified to give the dimensionless temperature at the centerline of the rod, the following equation results:

$$\begin{aligned} \theta &= \frac{T - T_\infty}{T_0 - T_\infty} \\ &= 2 \sum_{n=1}^{\infty} \frac{\text{Bi}}{J_0(\Gamma_n)(\Gamma_n^2 + \text{Bi}^2)} \exp(-\Gamma_n^2 r), \end{aligned} \quad (6)$$

where the eigenvalues Γ_n are roots of the equation:

$$\Gamma_n J_1(\Gamma_n) = Bi J_0(\Gamma_n), \tag{7}$$

and J_0 and J_1 are Bessel functions of order zero and one, respectively. For the range of Biot numbers studied, ten terms of the infinite series were determined to yield an accuracy of more than 5 significant digits in θ .

When the series in eq. (6) is truncated after the first term, the following equation is obtained:

$$\ln \theta' = \ln \left\{ \frac{2 Bi}{J_0(\Gamma_1)(\Gamma_1^2 + Bi^2)} \right\} - \Gamma_1^2 \tau. \tag{8}$$

In order to determine when the series could be truncated after the first term, the error in truncation had to be determined as a function of dimensionless time τ and Biot number. The relative truncation error was defined to be $(\theta' - \theta)/\theta$, where θ is the exact solution which was taken as the value of θ when the series was truncated after ten terms. The dimensionless time τ_{crit} beyond which the truncation error is less than 0.01 is plotted in fig. 1 for values of the Biot number between 0 and 0.9. For values of the Biot number between about 0.05 and 0.9, the critical dimensionless time is given by the 5th order polynomial fit:

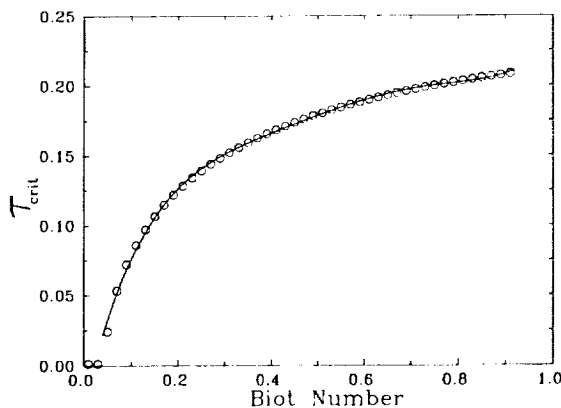


Fig. 1. The dimensionless time τ_{crit} versus Biot number past which the error in θ caused by truncation of eq. (6) after the first term is less than 0.01. The line represents the 5th order polynomial fit given by eq. (9).

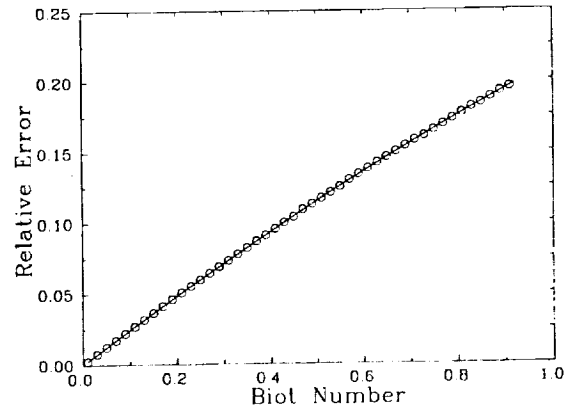


Fig. 2. Relative error caused by assuming the Biot number equals -0.5 times the slope of a $\ln \theta$ versus τ plot. The line represents the 2nd order polynomial fit given by eq. (10).

tionless time is given by the 5th order polynomial fit:

$$\tau_{crit} = 3.02 Bi^5 - 8.54 Bi^4 + 9.32 Bi^3 - 5.03 Bi^2 + 1.48 Bi - 0.0302. \tag{9}$$

Eq. (8) is accurate to within 1% in dimensionless temperature for dimensionless times greater than τ_{crit} . Therefore, a plot of $\ln \theta$ versus τ should be linear after time τ_{crit} . If a linear regression analysis is carried out on experimental data at dimensionless times greater than τ_{crit} , Γ_1 is given by the square root of the negative of the slope. This experimentally determined value of Γ_1 can then be used in eq. (7) to calculate the Biot number.

Eq. (8) is similar to the lumped-capacity solution, except that the intercept is not zero and the slope is $-\Gamma_1^2$ as compared to $-2 Bi$ from the lumped-capacity model. The validity of the lumped-capacity solution can be assessed by calculating the relative error caused by assuming the Biot number equals the negative of the slope of a $\ln \theta$ versus τ plot divided by two. The relative error can be defined as $(Bi - \Gamma_1^2/2)/Bi$, where Bi is the actual Biot number and Γ_1 is calculated from eq. (7). The relative error is plotted in fig. 2 as a function of Biot number and is given by the 2nd order polynomial fit:

$$\text{relative error} = -0.0373 Bi^2 + 0.248 Bi, \tag{10}$$

for Biot numbers between 0 and 0.9. The relative error is almost a linear function of Biot number in this region.

This analysis suggests that care must be taken when applying the lumped-capacity model to experimental data. A linear regression analysis should only be done for values of $\tau > \tau_{crit}$. When the Biot number is large, most of the temperature change could occur before τ_{crit} and the error in assuming the slope equals $-2 Bi$ becomes large. Also, the experimental error in temperature measurement causes large errors in the value of $\ln \theta$ when T approaches T_∞ . This is best demonstrated by example. Let us consider the case when $T_0 = 800^\circ\text{C}$, $T_\infty = 700^\circ\text{C}$, and the error in measurement of the object's temperature is 1°C . If the temperature of the object T is 750°C , the error in the resulting value of $\ln \theta$ is only 3%. However, when the temperature of the object is 701°C , the error is 15%. Another important point when applying the lumped-capacity model is that the straight line should not be forced through the origin. A two-parameter regression analysis should be performed, as suggested by eq. (8).

4. Experimental technique

The lumped-capacity method was demonstrated using an ampoule and thermocouple arrangement containing molten GaSb situated in the heater of a Bridgman-Stockbarger furnace at temperature T_0 . The ampoule was moved suddenly to a region of different temperature T_∞ . The temperature versus time data were collected as the melt equilibrated to the new temperature and the lumped-capacity model was used to determine the heat transfer coefficient between the ampoule and furnace.

The experimental apparatus consisted of a three-zone vertical Bridgman-Stockbarger furnace. The heating zones of the furnace were made of Kanthal heating elements embedded in Fibrothal insulation. The 5 cm long adiabatic zone was fabricated from zirconia insulation. Quartz tubing was used as a liner in the furnace. Two K-type thermocouples, inserted halfway into the heaters between the furnace wall and the liner,

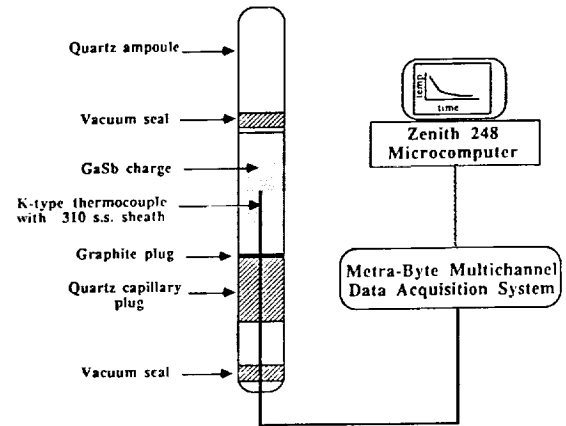


Fig. 3. Schematic diagram of ampoule and thermocouple arrangement with data acquisition system for in-situ temperature measurements.

were used for control. Both ends of the furnace were plugged to eliminate the chimney effect.

The 0.9 cm inner diameter and 1.1 cm outer diameter quartz growth ampoule, shown in fig. 3, was loaded with a 7 cm long GaSb charge, compounded from six-9s purity Ga and Sb in a rocking furnace for 5 h at 820°C . The temperature in the melt was measured using a 0.041 cm diameter grounded K-type thermocouple with a 310 stainless steel sheath and MgO as insulation (made by General Measurements). The tip of the thermocouple was positioned 3 cm into the ampoule at the center of the charge.

The molten charge was allowed to reach thermal equilibrium with the surroundings prior to each experiment. For experiments 1 and 2, the ampoule was suddenly moved from the lower zone to the upper zone and held firmly. While for experiment 3, the ampoule started in the upper zone and was moved to the lower zone. The thermocouple output was collected versus time using a data acquisition system.

5. Results

5.1. Experimental determination of heat transfer coefficients

Fig. 4 shows the actual thermocouple readings collected from the molten GaSb during experi-

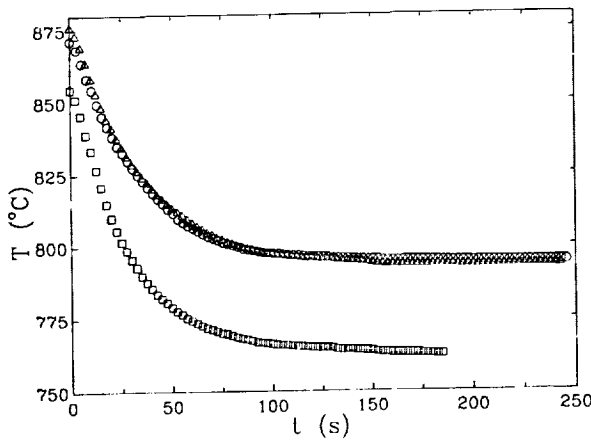


Fig. 4. Thermocouple readings in molten GaSb. The circles, triangles, and squares represent the data of experiments 1, 2, and 3, respectively.

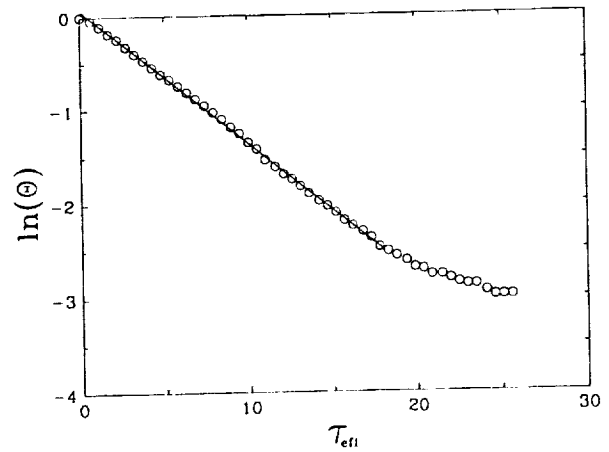


Fig. 5. Experimental data and the resulting linear fit ($R^2 = 0.9993$) for experiment 1.

ments 1, 2, and 3 (see also table 1). The logarithm of the dimensionless temperature θ was plotted versus dimensionless time τ_{eff} for each experiment. Linear regression analyses using NCSS Statistical Software were performed to determine the slopes and intercepts of these plots. The plot for experiment 1 is shown in fig. 5.

The linear regression analysis for experiment 1 was performed on the data for τ_{eff} between 0.1 and 18. There are two reasons that these limits for τ_{eff} were chosen. The value of τ_{crit} , beyond which the relationship between $\ln \theta$ and τ_{eff} is linear, is less than 0.1. Also, the experimental data tend to bend upward beyond $\tau_{eff} = 18$. The reason for this is the magnification of experimental error at small values of θ . (Both of these explanations are discussed fully in section 3). The resulting linear fit is $\theta = (-0.142 \pm 0.0006)\tau + (0.0697 \pm 0.0059)$. The uncertainty values are 95% confidence limits on

the slope and intercept, which can be transformed into 95% confidence limits on the Biot number. The lumped-capacity solution leads to a Biot number of 0.0712 ± 0.0003 determined from the slope. The value of the Biot number determined using the model accounting for radial temperature gradients is 0.0725 ± 0.0003 .

The same analysis as above was performed for experiments 2 and 3. The linear regression analysis for experiment 2 was performed on the data for τ_{eff} between 0.1 and 20. The linear fit is $\theta = (-0.138 \pm 0.0004)\tau + (0.0407 \pm 0.0042)$. The lumped-capacity solution leads to a Biot number of 0.0689 ± 0.0002 . The value of the Biot number determined using the model accounting for radial temperature gradients is 0.0701 ± 0.0002 . For experiment 3, the linear regression analysis was performed on the data for τ_{eff} between 0.1 and 15. The linear fit is $\theta = (-0.171 \pm 0.0008)\tau + (0.0522 \pm 0.0073)$. The lumped-capacity solution leads to a Biot number of 0.0855 ± 0.0004 . The value of the Biot number determined using the model accounting for radial temperature gradients is 0.0873 ± 0.0004 .

The heat transfer coefficients obtained for experiments 1, 2, and 3 are presented in table 2. There are two different values for each experiment. One is from the lumped-capacity model and one is from the model which accounts for radial temperature gradients.

Table 1
Listing of the temperatures of the upper zone T_u , lower zone T_l , the initial charge temperature T_0 , and final steady-state charge temperature T_∞ for experiments 1, 2, and 3

Experiment	Temperature ($^{\circ}\text{C}$)			
	T_u	T_l	T_0	T_∞
1	800	890	871	792
2	800	890	876	794
3	870	780	855	762

Table 2
Comparison of the experimentally determined and theoretically estimated values of the heat transfer coefficient for experiments 1, 2, and 3

Experiment	h (W/cm ² ·K)		
	Lumped-capacity model	Radial model	Theoretical estimation
1	0.0189	0.0193	0.0220
2	0.0183	0.0186	0.0220
3	0.0227	0.0232	0.0189

5.2. Theoretical estimation of heat transfer coefficients

The heat transfer coefficient between the ampoule wall and the furnace could also be estimated by a simple heat transfer formulation. The heat transfer coefficient is derived by summing the heat transfer by radiation and conduction through the air gap between the ampoule and the furnace wall in a concentric cylindrical system and equating it to the heat flux per unit area Q through the ampoule containing the growth materials:

$$Q = \bar{h}(T_h - T_a) = \sigma \epsilon F(T_h^4 - T_a^4) + \frac{k_{\text{air}}(T_h - T_a)}{R_a \ln(R_f/R_a)}. \quad (11)$$

The contribution of natural convection between the ampoule and the furnace was determined by computing the Grashof number in the air gap between the ampoule and the quartz liner. We estimated the Grashof number for our experiments to be 246 and concluded that the contribution of natural convection to the heat transfer was insignificant [10]. Therefore, the convective heat transfer term was not included in eq. (11).

The view factor $F = 0.9$ was approximated using the view factor for finite-length concentric cylinders (i.e. furnace-ampoule) [8]. The ampoule temperature T_a was assumed to be the same as the temperature of the molten charge, since the ampoule wall was only 0.1 cm thick compared to the 0.45 cm charge radius. The steady-state temperature reading in the charge T_∞ and the temper-

ature of the control thermocouple were used for T_a and T_h , respectively. The values of $T_a = 793^\circ\text{C}$ and $T_h = 800^\circ\text{C}$ for experiments 1 and 2, and $T_a = 762^\circ\text{C}$ and $T_h = 780^\circ\text{C}$ for experiment 3 were used in calculation of the heat transfer coefficients.

The values of \bar{h} calculated for experiments 1, 2, and 3 were 0.0220, 0.0220, and 0.0189 W/cm²·K, respectively. The estimated heat transfer coefficients are compared with the experimentally determined values in table 2.

6. Discussion

Fig. 6 depicts the comparison between the Biot numbers calculated from the lumped-capacity model ($\text{Bi} = -m/2$) and from the model including radial temperature gradients ($\Gamma_1 = \sqrt{-m}$, $\text{Bi} = \Gamma_1 J_1(\Gamma_1)/J_0(\Gamma_1)$). The horizontal and vertical lines in the figure represent 95% confidence limits on the values of the Biot number. The three data points would fall along the solid diagonal line if the results from the lumped-capacity model agreed exactly with the theory that considers radial temperature gradients in the charge. The dashed line

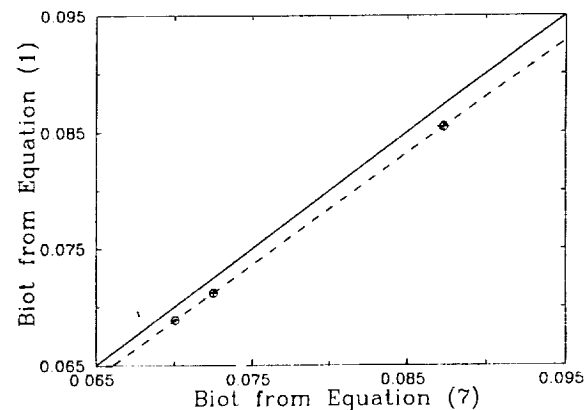


Fig. 6. Comparison between the Biot numbers calculated from the slope using eq. (1) (lumped-capacity model) and using eq. (7). The horizontal and vertical lines in the figure represent 95% confidence limits on the values of the Biot number. The dashed line represents the calculated relative error between the two models and is given by eq. (10).

represents the calculated relative error between the two models and is given by eq. (10).

The Biot numbers calculated from the model accounting for radial temperature gradients were greater than those calculated from the lumped-capacity model. The fact that the three data points fall on the dashed line proves the relationship between the lumped-capacity Biot number and the radial temperature gradient Biot number is satisfied exactly. If the Biot number is determined using the simple lumped-capacity model, the correct Biot number can be calculated by finding the root of the rearranged form of eq. (10):

$$f(\text{Bi}) = 0.0373 \text{Bi}^3 - 0.248 \text{Bi}^2 + \text{Bi} - \text{Bi}_L = 0, \quad (12)$$

for values of the Biot number between 0 and 0.9, where Bi_L is the Biot number calculated using the lumped-capacity model.

Experiments 1 and 2 were almost identical, yet the Biot numbers calculated from each differ by about 4%. This difference could have been caused by a change in the position of the charge within the furnace. The lengths of the heated zones were 15 cm, not overly long compared to the charge length of 7 cm. It is possible that one or both experiments were influenced by the charge being positioned in a region where the temperature changed with height in the furnace. This would cause axial temperature gradients in the melt that would violate the assumptions of the models used. However, the small difference in Biot numbers between experiments 1 and 2 is not significant when considering the fact that heat transfer coefficients depend continuously on position in a crystal growth furnace, and this technique was used to get an overall value for the heat transfer coefficient in a zone.

The Biot number calculated from experiment 3 was about 20% higher than those calculated from experiments 1 and 2. Experiments 1 and 2 measured the heat transfer coefficient in the upper zone, while experiment 3 measured that in the lower zone. The difference in heat transfer characteristics between the upper and lower zones was unexpected. These zones are constructed identically. The temperature drops as the bottom of the

lower zone is approached. This temperature gradient caused axial heat transfer which could have increased the heat transfer coefficient.

It is also probable that natural convection was present in the liquid during the experiments. However, the effect of natural convection would not be expected to be large in a low Prandtl number fluid like a semiconductor melt.

The values of the heat transfer coefficient calculated experimentally differ by 15% from simple theoretical estimations. This difference is quite small and could be due to inaccuracies in the values of emissivity and view factor.

7. Conclusions

A practical, experimental approach was developed to determine the average heat transfer coefficient between a charge and directional solidification furnace. It was determined that the lumped-capacity model is accurate in determining the Biot number within a relative error given by eq. (10) for Biot numbers between 0 and 0.9. However, this is only if the linear regression analysis on the $\ln \theta$ versus τ plot is carried out for values of $\tau > \tau_{\text{crit}}$, where τ_{crit} is given by eq. (9). The straight line fit should not be forced through the origin because the theory that accounts for radial temperature gradients predicts a slope and a non-zero intercept. For values of $\tau > \tau_{\text{crit}}$, the Biot number can be determined exactly by obtaining Γ_1 from the slope of a $\ln \theta$ versus τ plot. This value can then be used to calculate the Biot number from eq. (7).

The heat transfer coefficient between the ampoule and the furnace was estimated by a simple formulation accounting for conduction and radiation across the air gap. Remarkably, the results differ by only 15% from the values calculated by the lumped-capacity method.

Acknowledgement

This work was supported by NASA under grants NAG8-541 and NGT-50310.

Nomenclature

A	Surface area of the charge (17.3 cm ²)	T_h	Heater temperature (°C)
Bi	Biot number hR/k	T_l	Temperature of the lower furnace zone (°C)
Bi_{eff}	Effective Biot number between the charge and ampoule and the furnace, $\bar{h}_{eff}R_a/k_{eff}$	T_u	Temperature of the upper furnace zone (°C)
Bi_L	Biot number calculated by the lumped-capacity method	T_0	Initial temperature of charge (°C)
c_a	Specific heat capacity of the ampoule ($c_a = 1.19$ J/g · K at 1075 K for fused silica [11])	T_∞	Steady-state temperature of charge (°C)
c_c	Specific heat capacity of the molten GaSb charge calculated using thermal conductivity, thermal diffusivity, and density data (for GaSb 0.328 J/g · K)	V_a	Volume of the section of ampoule containing the charge; $V_a = \pi L(R_a^2 - R_c^2)$ (2.2 cm ³)
c_{eff}	Mass weighted average effective specific heat capacity of charge and ampoule combination, $c_{eff} = (\rho_c V_c c_c + \rho_a V_a c_a) / (\rho_c V_c + \rho_a V_a)$ (0.479 J/g · K for present experiments)	V_c	Volume of the charge (4.46 cm ³)
F	View factor from furnace wall to the ampoule (0.9 for present configuration)	α	Thermal diffusivity (cm ² /s)
h	Heat transfer coefficient (W/cm ² · K)	α_c	Thermal diffusivity of charge (0.087 cm ² /s for molten GaSb [12])
\bar{h}	Average heat transfer coefficient between the growth material and the furnace (W/cm ² · K)	α_{eff}	Effective thermal diffusivity of charge and ampoule (0.0628 cm ² /s)
\bar{h}_{eff}	Effective average heat transfer coefficient between the charge and ampoule and the furnace (W/cm ² · K)	Γ_n	n th eigenvalue
J_n	Bessel function of order n	ϵ	Emissivity of the furnace (for Kanthal $\epsilon = 0.75$ [15])
k	Thermal conductivity (W/cm · K)	θ	Dimensionless temperature $((T - T_\infty)/(T_0 - T_\infty))$
k_a	Thermal conductivity of ampoule ($2.42 \times 10^{-5}T + 4.48 \times 10^{-3}$ W/cm · K for fused silica [14], $k_a = 0.0308$ W/cm · K at $T = 1075$ K)	θ'	Dimensionless temperature calculated from eq. (8)
k_c	Thermal conductivity of the charge (0.171 W/cm · K for molten GaSb [12])	ρ_a	Density of ampoule wall, ($2.28 \times 10^{-4}T + 2.273$ g/cm ³ for fused silica [17], $\rho_a = 2.586$ g/cm ³ at 1075 K)
k_{eff}	Mass weighted effective thermal conductivity of charge and ampoule (0.146 W/cm · K)	ρ_{avg}	Average density of charge and ampoule, $\rho_{avg} = (\rho_c V_c + \rho_a V_a) / (V_c + V_a)$ (4.85 g/cm ³)
L	Length of the charge (7 cm)	ρ_c	Density of charge (5.98 g/cm ³ for molten GaSb at 800 °C [16])
m	Slope of linear equation	σ	Stefan-Boltzmann constant (5.67×10^{-12} W/cm ² · K ⁴)
Q	Heat flux per unit area through ampoule (W/cm ²)	τ	Dimensionless time ($\alpha t/R^2$)
R	Radius (cm)	τ_{crit}	Dimensionless time beyond which eq. (8) is valid
R_a	Outside radius of ampoule (0.55 cm)	τ_{eff}	Effective dimensionless time ($\alpha_{eff} t/R^2$)
R_c	The charge radius (0.45 cm)		
R_f	Inside radius of furnace (3.81 cm)		
t	Time (s)		
T	Temperature at time t (°C)		
T_a	Ampoule temperature (°C)		

References

- [1] C.E. Chang and W.R. Wilcox, J. Crystal Growth 21 (1974) 135.
- [2] T.W. Fu and W.R. Wilcox, J. Crystal Growth 48 (1980) 416.
- [3] F.M. Carlson, A.L. Fripp and R.K. Crouch, J. Crystal Growth 68 (1984) 747.
- [4] C.J. Chang and R.A. Brown, J. Crystal Growth 63 (1983) 343.
- [5] R.J. Naumann, J. Crystal Growth 58 (1982) 554.
- [6] P.C. Sukaneck, J. Crystal Growth 58 (1982) 208.
- [7] T.W. Fu, PhD Thesis, Clarkson University (1981).

- [8] M.N. Ozisik, Heat Transfer; A Basic Approach (McGraw-Hill, New York, 1985).
- [9] H.S. Carslaw and J.C. Jaeger, Conduction of Heat in Solids, 2nd ed. (Oxford University Press, London, 1959).
- [10] W.H. McAdams, Heat Transmission, 3rd ed. (McGraw-Hill, New York, 1954).
- [11] E.B. Shand, Glass Engineering Handbook, 2nd ed. (McGraw-Hill, New York, 1958).
- [12] A.S. Jordan, J. Crystal Growth 71 (1985) 551.
- [13] R.C. Weast, Handbook of Chemistry and Physics (CRC Press, Boca Raton, FL, 1986).
- [14] Y.S. Touloukian, R.W. Powell, C.Y. Ho and P.G. Klemens, Thermophysical Properties of Matter, Vol. 2, Thermal Conductivities (IFI/Plenum Data, New York, 1970).
- [15] Kanthal Corporation, Bethel, CT.
- [16] V.M. Glazov, S.N. Chizhorskaya and N.N. Glagoleva, Liquid Semiconductors (Plenum, New York, 1969).
- [17] Y.S. Touloukian, R.K. Kirby, R.E. Taylor and T.Y.R. Lee, Thermophysical Properties of Matter, Vol. 13, Thermal Expansion (IFI/Plenum Data, New York, 1973).